Review Article

Trendless Sequence as a New Source of Information: A Possibility to Present it in the Form of the Compact 3D-surface

RR Nigmatullin*, VS Alexandrov and RK Sagdiev

Radioelectronics and Informative-Measurement Technics Department, Kazan National Research Technical University (KNRTU-KAI) Named After A.N. Tupolev, Kazan, Tatarstan, Russian Federation

*Corresponding Author: RR Nigmatullin, Radioelectronics and Informative-Measurement Technics Department, Kazan National Research Technical University (KNRTU-KAI) Named After A.N. Tupolev, Kazan, Tatarstan, Russian Federation.

Abstract

In this paper the authors want to prove that the trendless sequences (TLS) can be transformed to 3D-surface having only 10 statistically-significant parameters. These ten parameters can be extracted from random noise with the help of the Comparative Analysis of Positive/Negative fluctuations (CAPoNeF) method. Actually, without using of a treatment error (usually accompanying any data treatment procedure) and imposed model assumptions one can form 10-measured feature space for comparison of one random sequence with another one. This feature space can be projected to the Euclidean 3D-space having 10 statistical parameters. Comparison of these parameters associated with different noise tracks allows to use this set of the parameters for selection and other purposes associated with "standard"/reference equipment. This combined method (CAPoNeF+3D-DGI) is applied for comparison of the TLS obtained for operational amplifiers. Another example is related to transformation of acoustic signals corresponding to a "calm", "tranquil" and "storming" waves, correspondingly. Not pretending to complete description of the considered data the authors want to show that the combined method is "universal" and can be used for analysis of different data. Thanks to high sensitivity of this combined method, we can compare filtered and non-filtered data and express the difference of 10 parameters in terms of the corresponding 3D-surfaces. This method can detect easily the differences between the compared waves and represent them in the form of the 3D-surfaces also. These surfaces are convenient for detecting the differences between initial TLS(s) and sequences having hidden trends that initially are similar to each other.

Keywords: Trendless Sequences (TLS); Combination of the 3D-Discrete Geometrical Invariants (DGI) and CAPoNeF Methods; Noise of Operational Amplifiers; Comparison of Acoustic Sea Waves of Different Intensity

Abbreviations

DGI: Discrete Geometrical Invariants; CAPoNeF.: Comparative Analysis of Positive and Negative Fluctuations; TLS: Trendless Sequence; OA: Operational Amplifier

Introduction

Nowadays a "noise" (oscillations of random fluctuations) becomes an important object of research. Before of fluctuations consideration, any random trend was considered as a response/reaction on some applied external field. This field could be mechanical, electromagnetic and etc. Then the theory tries to describe the obtained response and the coincidence of the fitting curve with the measured trend gives us a portion of definite information and, therefore, deeps the understanding of the surrounding world. In nowadays another tendency is observed. Scientists try to get an information from random fluctuations that earlier were considered as insignificant and useless "noise".

The idea that a random noise represents a source of information is not a new one. Part of the researchers try to extract an information based on some reasonable suppositions. In particular, the basics of the fluctuation noise spectroscopy (including also many useful references) are given in the book [1] and in papers [2,3]. The approach based on the Mori-Zwanzig formalism was given in the papers [4,5]. Unfortunately, these approaches include some unjustified suppositions and become useless in analysis of random sequences having different nature. These suppositions and their analysis are listed in paper [6]. The essential results were obtained from analysis of electro-chemical noise [7-12], other type of 'noises' associated with the earthquakes phenomenon and their quantitative description, medical data analysis is given in [3,4,13,14]. Unfortunately, in spite of these promising attempts the general picture associated with analysis of arbitrary types of random sequences (especially TLS) is far from an 'ideal' one. Researchers based on their own (and in many cases unjustified suppositions) try to process many types of random sequences and extract an 'information" mixed, unfortunately, with treatment/uncontrollable errors. Especially, they will have problems with analysis of equipment "noise" (pure TLS) that in many cases is not the Gaussian, uniform and other type of noises widely used in the mathematical statistics as model TLS(s). Therefore, for description of random fluctuations we need very accurate tool that is free from the model assumptions and treatment errors. Only experimental errors related to the equipment measurements and influence of different uncontrollable factors should be taken into account.

Therefore, there is an urgent task in creation of the reliable processing tool that (a) should be free from the treatment errors and (b) rather universal for application to any TLS(s) that are generated or contained in the given equipment. Only in this case we can compare the given type of fluctuations with other ones and select a calibration equipment based on the measurements of 'reference' data.

The basic problem that we are going to solve in this paper can be formulated as follows: we are trying to combine the merits and effectiveness of the CAPoNeF method [15] with a "fine" sensitivity and geometric visualization of 3D-DGI (Discrete Geometrical Invariants) surfaces [16]. Then this combined method will be applied for detection of the differences between filtered and unfiltered TLS(s) that were obtained from the operational amplifiers. One can show that initial rectangle matrix representing the initial TLS(s) measurements, where N(number of rows)× M(number of columns) can be transformed into the compact matrix (P = 10, number of parameters)×(E = 3, number of extreme values) that is represented by six 3D- surfaces, at least. These surfaces can be used as specific detectors for differentiation of the hidden factors that are "dissolved" in initial TLS(s).

This original combination is described in the Mathematical Appendices A and B. Another example is related to comparison of acoustic signals recorded for "calm", "tranquil" and "storming" Mediterranean Sea. The authors completely admit that they are not specialists in marine acoustics. However, the authors want to attract attention of the specialists working in the field of marine acoustics to this original method. To investigation of a random sea noise of different kind many papers are devoted. We can mark the papers [17-20] related to the influence of different factors on the dynamics of acoustic sea waves. However, the authors do hope that the proposed method given in this paper can find interesting applications in the modern marine acoustics, as well.

The content of the paper is organized as follows. In section 5.2.1 the experimental details are described related to measurements of the OA(s) noises. As the second example (section 5.2.2) we added the acoustic signals recorded for the Mediterranean Sea (waves in "calm", "tranquil/ordinary" and in the "storming" states, accordingly). In the same section we describe the signal processing procedure and analysis of data. In the final sections 6 and 7 we discuss the obtained results and outline the perspective of the further research. Some important details related to CAPoNeF and 3D-DGI methods are given in the Mathematical Appendices A and B.

Materials and Methods

Experimental setup

The scheme of the experimental setup is shown in Figure 1a and is generally accepted for connecting an operational amplifier. The nominal values of the components are selected from the condition of ensuring the best noise parameters of the system under study and in accordance with the recommendations of the manufacturer of the corresponding electronic chips. First of all, it was necessary to simulate the amplifier stage in the Multisim electronic environ-

Trendless Sequence as a New Source of Information: A Possibility to Present it in the Form of the Compact 3D-surface

25

The basic parameters of the CAPoNeF method

The CAPoNeF method described in paper [15] uses 10 key parameters that describe an arbitrary trendless noise. Here it is instructive to remind it again in order to combine them in one list.

$p_1 = \dfrac{1}{N}\sum_{j=1}^{N} y_j$ this parameter determines the mean value of the TLS that corresponds to a specific balance between positive and negative fluctuations.

$p_2 = Rg(Dy) = \max(Dy) - \min(Dy)$, this parameter defines the range of the given sequence, namely,

$Dy_j = y_j - N^{-1}\sum_{j=1}^{N} y_j$ $(j=1,2,...,N)$ This value is always positive and corresponds to the maximal intensity of the given TLS.

$p_3 = Rg(|Dy|) = \max(Dy_+) - |\min(Dy_-)|$ this parameter defines the relative contribution of amplitudes that are on the opposite sides of the TLS. When $Rg\,(|Dy|) \cong 0$ it corresponds to an "ideal" balance between positive and negative amplitudes. In the opposite case, when $Rg\,(|Dy|) < (>) 0$, we observe specific "spikes/outliers" of positive (negative) amplitudes in the given TLS relatively to each other. $p_4 = Rg(Sm(y)) = \max(Sm_+) - \min(Sm_-)$, $Sm_{\pm} = \sum_{j=1}^{N_{\pm}} Dy_{j,\pm}$ which defines the range of sums that evaluates the cumulative effect of the given fluctuations. It is proved to be very effective together with the independent parameter p_2. For "ideal" TLS this value together with p_2 should be minimal.

$p_5 = Sm = \langle y \rangle - 0.5 \cdot (\max(y) - \min(y))$, which reflects a possible asymmetry between positive and negative fluctuations with respect to their mean value. If $p5$ is close to zero, then one concludes that the TLS is completely symmetric, in other cases ($p_5 < 0,\, or\, p_5 > 0$) it is possible to assess the value of asymmetry.

$p_6 = DN_{\pm} = Nx_+ - Nx_-$, which determines the number of amplitudes located in the opposite sides of the TLS. If ($p_6 < 0,\, or\, p_6 > 0$) then the number of positive amplitudes exceeds the number of negative amplitudes or vice versa.

$p_7 = \max(Bd)$. If all amplitudes of the initial TLS – yj are put in descending order ($y1 > y2 > ... > yN$) and the obtained sequence of these ranged amplitudes is integrated, then one receives the bell-like curve defined by $Bd(x; \alpha, \beta, A) = A(x - x_0)^{\alpha}(x_N - x)^{\beta}$ and the maximum of this integrated curve clearly indicates the boundary between positive and negative fluctuations.

$p_8 = Range(J(Dy)) = \max(J(Dy)) - \min(J(Dy))$, which reflects the range of the cumulative fluctuations that are obtained after summation of positive and negative fluctuations, where $DJ_j = DJ_{j-1} + y_j$, $DJ_0 = 0$, $j=1,2,...,N$. N is the number of samples in the considered sequence. The minimal value of this parameter signifies about the minimal range/stability of the given fluctuations.

$p_9 = \langle (J(Dy)) \rangle$, the mean value of the curve $J(Dy)$ is also important for evaluating the contribution of the cumulative fluctuations.

$p_{10} = \langle \omega \rangle$, which is an important parameter to determine the mean frequency of the fluctuations that cross the horizontal axis. In the most cases, the distribution of the roots can be approximated by a segment of the straight line $rk \cong a.k + b$, where the integer value k determines the number of the calculated roots. In this simple case, the mean frequency $\langle \omega \rangle$ and the corresponding

$\cos\left(\langle \omega \rangle r_k - \langle \varphi \rangle\right) = 0$, or, equivalently $\langle \omega \rangle \cdot r_k - \langle \varphi \rangle = \dfrac{\pi}{2} + \pi k$.

The physical meaning of the parameter of $p10$ is the following. The higher value of this parameter signifies about the degree of "uniformity" of the given TLS to a "white noise" and vice versa. The minimal value of $\langle \omega \rangle$ informs about the predominant influence of low-frequency fluctuations.

These 10 parameters can characterize a specific "competition" between positive and negative fluctuations. These parameters are almost independent from each other and tends to minimal values if the considered TLS tends to stable state.

How to combine these parameters with other 10 parameters that characterize the 3D-Discrete Geometrical Invariant (DGI) that was described in paper [16]? The answer is given below in Appendix B.

Trendless Sequence as a New Source of Information: A Possibility to Present it in the Form of the Compact 3D-surface

26

Derivation of the 3D-DGI(s) surfaces

We remind that the Discrete Geometrical Invariants (DGI) in 3D space [16] is derived from any arbitrary chosen 3N data points forming the complete fourth order form including three variables can be reduced to 13 independent parameters forming the feature space of the corresponding dimension. These parameters including the desired combinations of the integer moments and their correlations up to the fourth order inclusive are proved to be very sensitive and general in order to compare one random sequence with another one. Besides, these 13 parameters extracted from the considered random sequence represent themselves a specific "fingerprint" for observing the evolution of random sequence in time or against another external factor as concentration, electromagnet/acoustic field intensity etc., in 3D space. This reduction procedure reminds a procedure used in the statistical mechanics when with the help of theGibbs partition function 3N trajectories of the microscopic particles are reduced to a finite set of thermodynamic parameters. Actually, the 3D-DGI(s) method realizes a similar procedure, i.e., it reduces 3N combination of an arbitrary random data points to 13 quantitative parameters forming the specific feature space. We want to stress here that this reduction procedure does not use any model and actually it is "universal". Besides, it does not contain any treatment errors as well and keeps only the measurement errors. Let us consider the completer power-law form of the 4-th order:

$$
\begin{aligned}
L_k^{(4)} &= A_{40}^{(1,0)}\left(y_1 - r_{1k}\right)^4 + A_{40}^{(2,0)}\left(y_2 - r_{2k}\right)^4 + A_{40}^{(3,0)}\left(y_3 - r_{3k}\right)^4 - \\
&- B_{22}^{(1,2)}\left(y_1 - r_{1k}\right)^2 \cdot \left(y_2 - r_{2k}\right)^2 - B_{22}^{(1,3)}\left(y_1 - r_{1k}\right)^2 \cdot \left(y_3 - r_{3k}\right)^2 - \\
&- B_{22}^{(2,3)}\left(y_2 - r_{2k}\right)^2 \cdot \left(y_3 - r_{3k}\right)^2 + \\
&+ C_{211}^{1(2,3)}\left(y_1 - r_{1k}\right)^2 \cdot \left(y_2 - r_{2k}\right) \cdot \left(y_3 - r_{3k}\right) + \\
&+ C_{211}^{2(1,3)}\left(y_2 - r_{2k}\right)^2 \cdot \left(y_1 - r_{1k}\right) \cdot \left(y_3 - r_{3k}\right) + \\
&+ C_{211}^{3(1,2)}\left(y_3 - r_{3k}\right)^2 \cdot \left(y_1 - r_{1k}\right) \cdot \left(y_2 - r_{2k}\right) - \\
&- \frac{1}{2} D_{31}^{(1,2)}\left(y_1 - r_{1k}\right) \cdot \left(y_2 - r_{2k}\right)\left[\left(y_1 - r_{1k}\right)^2 + \left(y_2 - r_{2k}\right)^2\right] - \\
&- \frac{1}{2} D_{31}^{(1,3)}\left(y_1 - r_{1k}\right) \cdot \left(y_3 - r_{3k}\right)\left[\left(y_1 - r_{1k}\right)^2 + \left(y_3 - r_{3k}\right)^2\right] - \\
&- \frac{1}{2} D_{31}^{(2,3)}\left(y_2 - r_{2k}\right) \cdot \left(y_3 - r_{3k}\right)\left[\left(y_2 - r_{2k}\right)^2 + \left(y_3 - r_{3k}\right)^2\right].
\end{aligned}
$$

(B1)

In expression (B1) the upper indices define the combination of the variables $y\alpha$ ($\alpha=1,2,3$) fixing the location of an arbitrary point $M(y_1,y_2,y_3)$ in 3D-space, the low indices determine the values of the power-law exponents that correspond to the algebraic form of the fourth order. The choice of the sign combination ($\pm$) before the constants in (B1) will be explained below. Three random sequences are determined by the values rak ($\alpha=1,2,3$; $k=1,2,…,N$). Expression (B1) represents itself the complete form of the fourth order that contains the combination of three variables associated with an arbitrary point $M(y_1,y_2,y_3)$ and three arbitrary sequences rak. The desired DGI is obtained from the following requirement

$$
\frac{1}{N}\sum_{k=1}^{N} L_k^{(4)} = I_4 .
$$

(B2)

In order to remove in expression (B2) the cubic terms we introduce the variables

$$
Y_\alpha = y_\alpha - \langle r_\alpha \rangle, \quad \langle r_\alpha \rangle = \frac{1}{N}\sum_{k=1}^{N} r_{\alpha k},
$$

(B3)

and nullify the linear terms. This requirement helps us to separate the desired variables $Y\alpha$ from each other and keep only the terms of the second and fourth orders, correspondingly. In order to decrease the number of constants in (B2) and derive the DGI not depending on some additional constants one defines three keyratio constants $R^{(\alpha,\beta)}$, where $(\alpha,\beta) = (1,2), (1,3), (2,3)$

$$
R^{(\alpha,\beta)} = \frac{B^{(\alpha,\beta)}}{A} = \frac{C^{\gamma(\alpha,\beta)}}{A} = \frac{D^{(\alpha,\beta)}}{A},
$$
$$
A_{40}^{(\alpha)} = A_{40}^{(\beta)} = A_{40}^{(\gamma)} \equiv A, \ \alpha,\beta,\gamma = 1,2,3.
$$

(B4)

It is convenient also to introduce the following notations for the integer moments and theirintercorrelations and present them in the form

$$
Q_{\alpha^m\beta^n\gamma^l} = \frac{1}{N}\sum_{k=1}^{N}\left(\left(\Delta r_{3k}\right)^m \left(\Delta r_{2k}\right)^n \left(\Delta r_{1k}\right)^l\right) \equiv \left\langle \left(\Delta r_\alpha\right)^m \left(\Delta r_\beta\right)^n \left(\Delta r_\gamma\right)^l \right\rangle,
$$
$$
\alpha \geq \beta \geq \gamma, (\alpha,\beta,\gamma) = 1,2,3.
$$

(B5)

In the result of the introduced notations (B4) and (B5), the system of linear equations for the finding of unknown ratios $R^{(\alpha,\beta)}$ from the nullification requirement of the entering linear terms accepts the form

Trendless Sequence as a New Source of Information: A Possibility to Present it in the Form of the Compact 3D-surface

27

$$\left[2Q_{221} - Q_{332} + \frac{3}{2}Q_{211} + \frac{1}{2}Q_{222}\right] \cdot R^{(1,2)} +$$

$$+ \left[2Q_{331} - Q_{322} + \frac{3}{2}Q_{311} + \frac{1}{2}Q_{333}\right] \cdot R^{(1,3)} - 2Q_{321} \cdot R^{(2,3)} = 4Q_{111},$$

$$\left[2Q_{211} - Q_{331} + \frac{3}{2}Q_{221} + \frac{1}{2}Q_{111}\right] \cdot R^{(1,2)} - 2Q_{321} \cdot R^{(1,3)} +$$

$$+ \left[2Q_{332} - Q_{311} + \frac{3}{2}Q_{322} + \frac{1}{2}Q_{333}\right] \cdot R^{(2,3)} = 4Q_{222},$$

$$-2Q_{321} \cdot R^{(1,2)} + \left[2Q_{311} - Q_{221} + \frac{3}{2}Q_{331} + \frac{1}{2}Q_{111}\right] \cdot R^{(1,3)} +$$

$$+ \left[2Q_{322} - Q_{211} + \frac{3}{2}Q_{332} + \frac{1}{2}Q_{222}\right] \cdot R^{(2,3)} = 4Q_{333}.$$

(B6)

The linear system of equations helps to reduce 3 moments (Q_{333}, Q_{222}, Q_{111}) and 7 intercorrelations of the third order (Q_{332}, Q_{322}, Q_{221}, Q_{211}, Q_{331}, Q_{311}, Q_{321}) to calculation of three unknown ratios $R^{(\alpha,\beta)}$ only. We should notice also that the combination of the algebraic signs in (A1) is chosen in that way for the keeping of the partial solution R=1 of system (B6) in the case when all three random sequences rak is identical to each other, i.e. $r_{1k} = r_{2k} = r_{3k}$. It is natural to define it as the case of spherical symmetry. If only two sequences coincide with other (for example, $r_{1k} = r_{2k} \neq r_{3k}$) i.e., we deal with the case of the cylindrical symmetry, then the linear system (6) is reduced to the couple of linear equations relatively the variables $R^{(1,2)} \neq R^{(1,3)} = R^{(2,3)}$. The number of triple correlations equals four in this case (Q_{111}, Q_{113}, Q_{133}, Q_{333}).

The system of equations (B6) facilitates considerably the further calculations. After averaging procedure applied to expression (B2) the structure of the fourth order form can be rewritten as $K_4(Y_1,Y_2,Y_3) + K_2(Y_1,Y_2,Y_3) = I_4$

(B7)

We chose the value of the invariant I4 as the double value of the free constant figuring in the left- hand side of (B7). After some algebraic manipulations the fourth and the second order forms entering to the left-hand side can be presented as

$$K_4(Y_1,Y_2,Y_3) = Y_1^4 + Y_2^4 + Y_3^4 + R^{(1,2)}Y_1Y_2\left[Y_3^2 - \frac{1}{2}(Y_1 + Y_2)^2\right] +$$

$$+ R^{(1,3)}Y_1Y_3\left[Y_2^2 - \frac{1}{2}(Y_1 + Y_3)^2\right] + R^{(2,3)}Y_2Y_3\left[Y_1^2 - \frac{1}{2}(Y_2 + Y_3)^2\right]$$

(B8a)

$$K_2(Y_1,Y_2,Y_3) = A_{11}Y_1^2 + A_{22}Y_2^2 + A_{33}Y_3^2 +$$

$$+ A_{12}Y_1Y_2 + A_{13}Y_1Y_3 + A_{23}Y_2Y_3.$$

(B8b)

The Constants $A_{\alpha\beta}$ figuring in expression (B8b) are defined as

$$A_{11} = 6Q_{11} - \left(Q_{22} + \frac{3}{2}Q_{21}\right)R^{(1,2)} - \left(Q_{33} + \frac{3}{2}Q_{31}\right)R^{(1,3)} + Q_{32}R^{(2,3)},$$

$$A_{22} = 6Q_{22} - \left(Q_{11} + \frac{3}{2}Q_{21}\right)R^{(1,2)} + Q_{31}R^{(1,3)} - \left(Q_{33} + \frac{3}{2}Q_{32}\right)R^{(2,3)},$$

$$A_{33} = 6Q_{33} + Q_{21}R^{(1,2)} - \left(Q_{11} + \frac{3}{2}Q_{31}\right)R^{(1,3)} - \left(Q_{22} + \frac{3}{2}Q_{32}\right)R^{(2,3)},$$

$$A_{12} = -\left(4Q_{21} + \frac{3}{2}Q_{11} + \frac{3}{2}Q_{22} - Q_{33}\right)R^{(1,2)} + 2Q_{32}R^{(1,3)} + 2Q_{31}R^{(2,3)},$$

$$A_{13} = 2Q_{32}R^{(1,2)} - \left(4Q_{31} + \frac{3}{2}Q_{11} + \frac{3}{2}Q_{33} - Q_{22}\right)R^{(1,3)} + 2Q_{12}R^{(2,3)},$$

$$A_{23} = 2Q_{31}R^{(1,2)} + 2Q_{21}R^{(1,3)} - \left(4Q_{32} + \frac{3}{2}Q_{22} + \frac{3}{2}Q_{33} - Q_{11}\right)R^{(2,3)}.$$

(B9)

The Constant I_4 (defined by 3 moments and 12 intercorrelations of the fourth order) figuring in theright-hand side of (B7) is defined as

$$I_4 = Q_{1111} + Q_{2222} + Q_{3333} - \left(Q_{2211} - Q_{3321} + \frac{1}{2}Q_{2111} + \frac{1}{2}Q_{2221}\right)R^{(1,2)} -$$

$$- \left(Q_{3311} - Q_{3221} + \frac{1}{2}Q_{3111} + \frac{1}{2}Q_{3331}\right)R^{(1,3)} -$$

$$- \left(Q_{3322} - Q_{3211} + \frac{1}{2}Q_{3222} + \frac{1}{2}Q_{3332}\right)R^{(2,3)}.$$

(B10)

It is interesting to notice that in the case of the spherical symmetry ($r_{1k} = r_{2k} = r_{3k}$) all correlations coincidewith each other and the value of I4 equals zero. The form of the fourth order (B7) admits the separation of the variables in the spherical system of coordinates. If one accepts the conventional notations:

$$y_1 = \langle y_1 \rangle + R\sin\theta\cos\varphi,$$

$$y_2 = \langle y_2 \rangle + R\sin\theta\sin\varphi,$$

$$y_3 = \langle y_3 \rangle + R\cos\theta,$$

$$0 \leq \theta \leq \pi, 0 \leq \varphi \leq 2\pi,$$

(B11)

then substitution of these variables into (B7) leads to the following biquadratic equation relatively the unknown radius R(θ,ф)

$$[R(\theta,\varphi)]^4 + \left(\frac{P_2(\theta,\varphi)}{P_4(\theta,\varphi)}\right)[R(\theta,\varphi)]^2 - \frac{I_4}{P_4(\theta,\varphi)} = 0.$$

(B12a)

The desired solution (R(θ, ф) > 0) is written as

Trendless Sequence as a New Source of Information: A Possibility to Present it in the Form of the Compact 3D-surface

28

$$R(\theta,\varphi) = \left[\frac{\sqrt{P_2^2(\theta,\varphi) + 4I_4 \cdot P_4(\theta,\varphi)} - P_2(\theta,\varphi)}{2P_4(\theta,\varphi)} \right]^{\frac{1}{2}}$$

(B12b)

The polynomials $P_{2,4}(\theta,\varphi)$ entering in (B12) are defined by the following expressions

$$P_4(\theta,\varphi) = \sin^4\theta \cdot \cos^4\varphi + \sin^4\theta \cdot \sin^4\varphi + \cos^4\theta +$$

$$+ R^{(1,2)} \sin^2\theta \sin\varphi \cos\varphi \left[\cos^2\theta - \frac{\sin^2\theta}{2}(\sin\varphi + \cos\varphi)^2 \right] +$$

$$+ R^{(1,3)} \sin\theta \cos\theta \cos\varphi \left[\sin^2\theta \sin^2\varphi - \frac{1}{2}(\sin\theta \cos\varphi + \cos\theta)^2 \right] +$$

$$+ R^{(2,3)} \sin\theta \cos\theta \sin\varphi \left[\sin^2\theta \cos^2\varphi - \frac{1}{2}(\sin\theta \sin\varphi + \cos\theta)^2 \right]$$

(B13a)

$$P_2(\theta,\varphi) = A_{11}\sin^2(\theta)\cos^2(\varphi) + A_{22}\sin^2(\theta)\sin^2(\varphi) + A_{33}\cos^2(\theta) +$$

$$+ A_{12}\sin^2(\theta)\sin(\varphi)\cos(\varphi) + A_{13}\sin(\theta)\cos(\theta)\cos(\varphi) + A_{23}\sin(\theta)\cos(\theta)\sin(\varphi).$$

(B13b)

The last expressions (B11)-(B13) determine the final form of the DGI in 3D-space. It includes three surfaces determined by expressions (B11). The further analysis shows that expression (B12b) equals zero (because $I_4 = 0$) in the case of the coincidence of three compared random sequences ($r_{1k} = r_{2k} = r_{3k}$). The radius $R(\theta,\varphi)$ can contain the complex expression when the integrand in (B12b) becomes negative. It accepts the negative values when the constant I_4 in the most cases defined by expression (B10) becomes negative. In this case, it is convenient to rewrite expressions (B11) in the form

$$y_1 = \langle y_1 \rangle + |R(\theta,\varphi)| \sin\theta \cos\varphi,$$

$$y_2 = \langle y_2 \rangle + |R(\theta,\varphi)| \sin\theta \sin\varphi,$$

$$y_3 = \langle y_3 \rangle + |R(\theta,\varphi)| \cos\theta,$$

$$|R(\theta,\varphi)| = \sqrt{\text{Re}(R^2(\theta,\varphi)) + \text{Im}(R^2(\theta,\varphi))},$$

$$0 \leq \theta < \pi, \ 0 \leq \varphi < 2\pi.$$

(B14a)

Three other imaginary" surfaces (when $I_4 < 0$) can be necessary for more detailed analysis

$$Y_1 = \text{Im}(R(\varphi,\theta))\cos(\varphi)\sin(\theta),$$

$$Y_2 = \text{Im}(R(\varphi,\theta))\sin(\varphi)\sin(\theta),$$

$$Y_3 = \text{Im}(R(\varphi,\theta))\cos(\theta)$$

$$0 \leq \varphi < 2\pi, \ 0 \leq \theta < \pi.$$

(B14b)

For convenience of a potential reader, we reproduce the basic

expressions that will help us to combine these two methods. Attentive analysis shows that 3 parameters $R^{(\alpha,\beta)}$ derived from the system (B6) and corresponding to correlations of the third order, enter only in the polynomials of the $P_4(\theta,\varphi)$ from (B13a). Six correlations of the second order enter only to polynomial of the second order $P_2(\theta,\varphi)$ from (B13b). Therefore, if one adds the invariant of the 4-th order from (B10) then we obtain 10 parameters then can be identified with 10 parameters following from the CAPoNeF method. Based on these 10 parameters one can determine only one surface for $R(\theta,\varphi)$ that is defined by relationship (B12b). We want to stress here that the 3D-DGI method is turned to be very flexible because it allows to use any 10 or 13 parameters (irrespective of their obtained sources) for construction of the desired 3D-surface in the significance space of the chosen parameters. We want to stress here again that the final expressions (B14) and (B15) do not use any model assumptions and are determined completely by the measured data together with their measurement errors only.

Trendless Sequence as a New Source of Information: A Possibility to Present it in the Form of the Compact 3D-surface

29

ment for a preliminary assessment of the correctness of the choice of the values of the corresponding components. This preliminary analysis showed high accuracy of the system functioning. This is necessary, among other things, in order to get a theoretical understanding of the behavior of our system.

The next task was to carry out measurements (Figure 1b-1d). When measuring several computing components (devices, sensors, chips), there are two possible connection schemes - serial and parallel. In our work, we applied the first method in which the signals from each sensor are taken in turn. In this case, there is a problem of ensuring the identity of external conditions (temperature, pressure, humidity, illumination, etc.), as well as to exclude the influence of the experimental installation itself on the sensor output signals.

Data processing took place in the LabVIEW program manufactured by National Instruments (it is worth noting that Elvis was developed by the same company, which ensures their full compatibility). The built-in ELVIS was used as an ADC with a sampling rate of 1.25 MS/s and a resolution of 16 bits. The application of the filtration procedure allowed to eliminate interfering factors and obtain smoother results. The filtration range was determined experimentally.

The diagram of the assembled experimental setup using the ELVIS working platform is shown below in Figure 1a. The study was conducted as follows. Amplifier noise was measured alternately using the board shown in Figure 1b, the results were recorded in the program. Each measurement was carried out with a small time interval to give the transistors a "rest" and cool down. To exclude external influences, the measuring board was closed with a metal box. To exclude external interference, the installation (including the metal box) was grounded (Figure 1c).

Signal processing procedure and the proposed algorithm
The differentiation of filtered and non-filtered data recorded for the OAs

In this section, we want to compose the merits of two methods described in the Mathematical Appendices A and B. A typical noise, recorded from the chip mentioned in the previous section is shown in figure 2. The basic aim of the treatment procedure is to find significant differences between nonfiltered and filtered data. The treatment algorithm is simple.
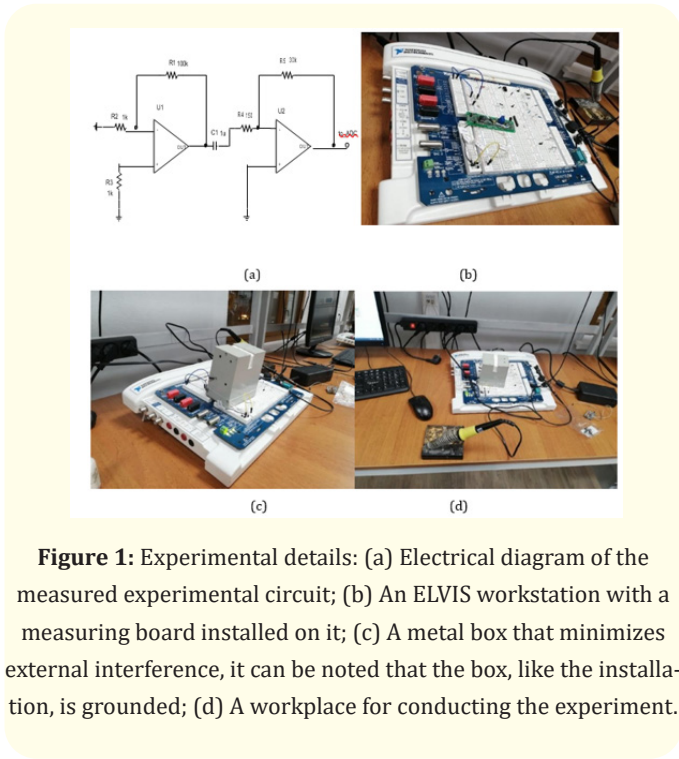
Figure 1: Experimental details: (a) Electrical diagram of the measured experimental circuit; (b) An ELVIS workstation with a measuring board installed on it; (c) A metal box that minimizes external interference, it can be noted that the box, like the installation, is grounded; (d) A workplace for conducting the experiment.
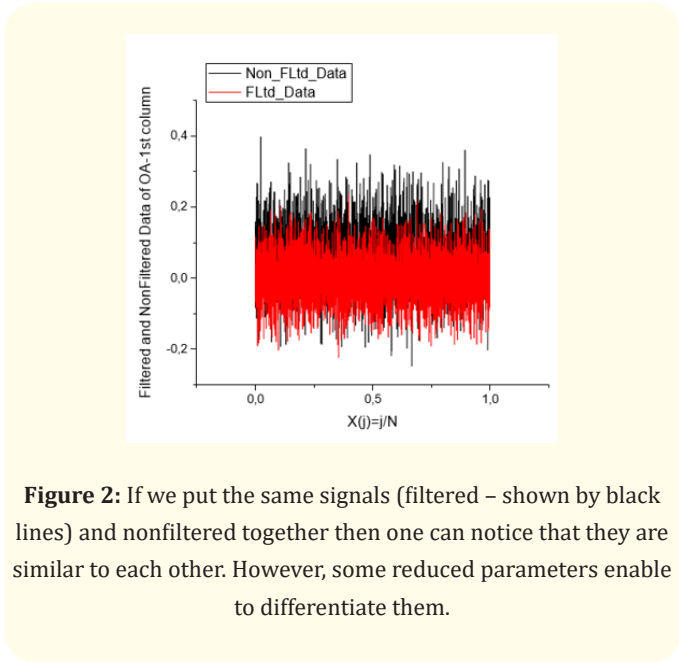
Figure 2: If we put the same signals (filtered – shown by black lines) and nonfiltered together then one can notice that they are similar to each other. However, some reduced parameters enable to differentiate them.

Based on the CAPoNeF method one transforms the initial data represented in the form of N×M rectangle matrix to the 10 parameters p1-p10. In the result of this transformation, we obtain the reduced matrix P×M.

The second stage is to extract only three extreme parameters from all set of columns (max(M), mean(M), min(M), where M counts all possible columns. In the result of this simple procedure we obtain the reduced matrix P (p = 1,2,...,10) × E (max(M), mean(M), min(M)) of the size (10´3). These 2 reduced matrices obtained for the OA(s) are shown in tables 1 and 2.

Maximal values	Mean values	Minimal values
p1 = 2.85200×10^{-1}(-1)	1.35413×10^{-1}(-1)	5.50126×10^{-2}(-2)
p2 = 7.30000×10^{-1}(-1)	6.44033×10^{-1}(-1)	5.65000×10^{-1}(-1)
p3 = 6.49470×10^{-2}(-2)	-3.25919×10^{-3}(-3)	$-7.29551 \times 10^{-2} \cdot$(-2)
p4 = 2.23135×10^{2}(2)	2.15190×10^{2}(2)	$2.03618 \times 10^{2} \cdot$(2)
p5 = -2.05498×10^{-2}(-2)	-1.86604×10^{-1}(-1)	$-3.09987 \times 10^{-1} \cdot$(-1)
p6 = 5.80000×10^{1}(1)	7.86667×10^{0}(0)	$-6.20000 \times 10^{1} \cdot$(1)
p7 = 3.72541×10^{-2}(-2)	3.59329×10^{-2}(-2)	$3.39970 \times 10^{-2} \cdot$(-2)
p8 = 5.84421×10^{0}(0)	4.99724×10^{0}(0)	$4.38371 \times 10^{0} \cdot$(0)
p9 = 1.19130×10^{0}(0)	-2.78621×10^{-1}(-1)	$-1.66859 \times 10^{0} \cdot$(0)
p10 = 4.19437×10^{3}(3)	3.88713×10^{3}(3)	$3.71354 \times 10^{3} \cdot$(3)

Table 1: Reduced Table that it was obtained for nonfiltered data.

Maximal values	Mean values	Minimal values
p1 = $3.80768 \, 10^{-5}$ (-5)	$-1.29759 \, 10^{-6}$ (-6)	$-5.48296 \, 10^{-5}$ (-5)
p2 = $6.14000 \, 10^{-1}$ (-1)	$5.21533 \, 10^{-1}$ (-1)	$4.59000 \, 10^{-1}$ (-1)
p3 = $6.99778 \, 10^{-2}$ (-2)	$1.06026 \, 10^{-2}$ (-2)	$-5.60384 \, 10^{-2}$ (-2)
p4 = $1.83841 \, 10^{2}$ (2)	$1.75657 \, 10^{2}$ (2)	$1.66191 \, 10^{2}$ (2)
p5 = $-2.29471 \, 10^{-1}$ (-1)	$-2.60768 \, 10^{-1}$ (-1)	$-3.06981 \, 10^{-1}$ (-1)
p6 = $5.00000 \, 10^{1}$ (1)	$-1.60000 \, 10^{0}$ (0)	$-6.20000 \, 10^{1}$ (1)
p7 = $3.07007 \, 10^{-2}$ (2)	$2.93319 \, 10^{-2}$ (-2)	$2.77471 \, 10^{-2}$ (-2)
p8 = $1.14964 \, 10^{0}$ (0)	$8.89650 \, 10^{-1}$ (-1)	$7.55824 \, 10^{-1}$ (-1)
p9 = $3.31283 \, 10^{-1}$ (-1)	$-7.57355 \, 10^{-3}$ (-3)	$-3.02367 \, 10^{-1}$ (-1)
p10 = $5.01350 \, 10^{3}$ (3)	$4.87626 \, 10^{3}$ (3)	$4.66314 \, 10^{3}$ (3)

Table 2: Reduced Table that it was obtained for filtered data.

Comments to the Tables. The first six parameters are related to correlations of the second order, other three parameters p7-p9 are associated with correlations of the third order and, finally, p10 is associated with the correlations of the 4-th order.

It is interesting to know which part of the number [Nm = e×10^{d}] (order of the number d or its mantissa e (having 5 significant digits) is the most significant in construction of the 3D-DGI surface. Actually, for each column in Tables 1,2 one can receive two surfaces that can be used for differentiation of filtered noise from unfiltered. The first six parameters p1-p6 will be used for calculations of the correlations of the second order, then parameters p7-p9 determine the correlations of the third order and, finally, the last parameter p10 is associated with the correlations of the 4-th order. We cannot show all 2(e,d)´3(E- columns)´2(nonfltd/fltd) = 12 surfaces. Attentive analysis shows that the surfaces based on the usage of the orders 10^{d} can differentiate easily the (non) filtered data from each other. See Figures. 3-10 for comparison. One can notice that the maximal and minimal values of the surfaces are more significant; they detect easily the difference between non-filtered and filtered data. One can notice also that the order of a number is more sensitive in comparison of its mantissa.
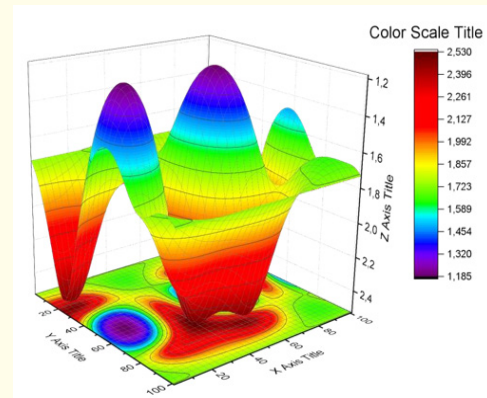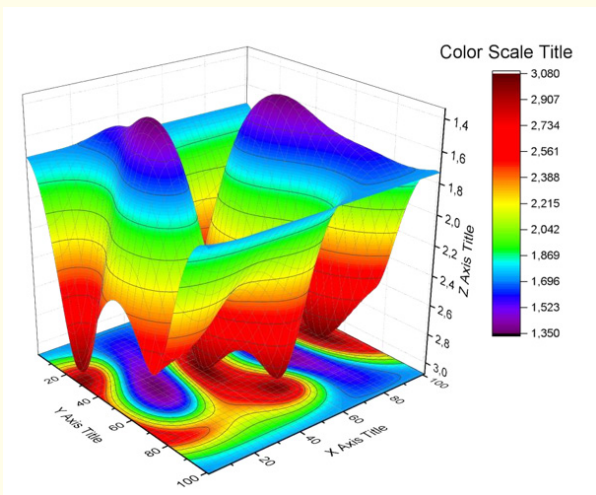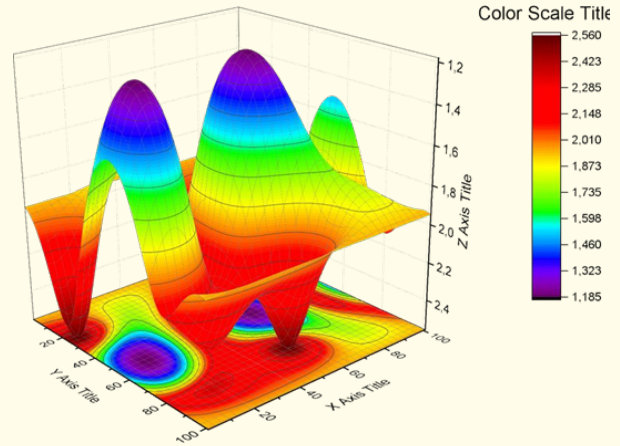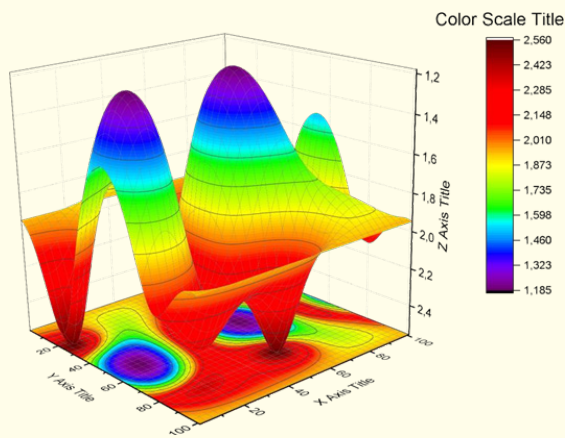

Figure 3: This surface is used the orders of max values corresponding to the nonfiltered data.

Trendless Sequence as a New Source of Information: A Possibility to Present it in the Form of the Compact 3D-surface
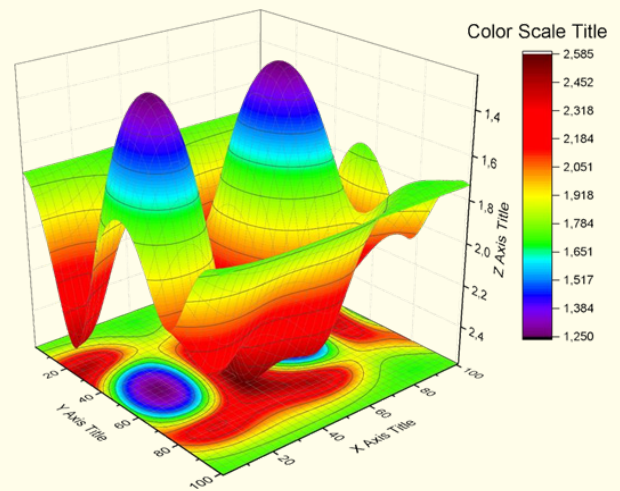
31

Figure 4: This surface based on the orders of maximal values corresponding to the filtered data. Comparison this surface with the previous one shows that they are different.
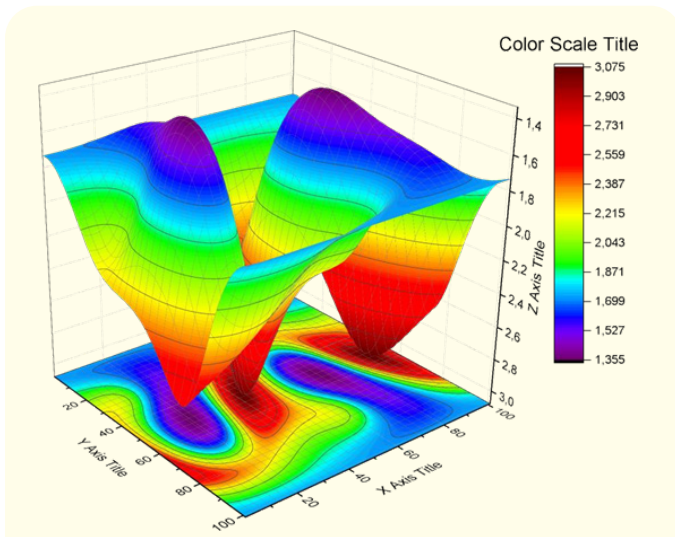

Figure 6: This surface is used the orders of mean values corresponding to the filtered data. If one can compare these two surfaces one can notice that these surfaces are identical and cannot differentiate the differences between filtered and non-filtered data.

Figure 5: This surface is used the orders of mean values corresponding to the non-filtered data.

Figure 7: This surface is used the orders of minimal values corresponding to the non-filtered data.

Figure 8: This surface is used the orders of minimal values corresponding to the filtered data. Comparison of the last two surfaces shows that they are quite different.

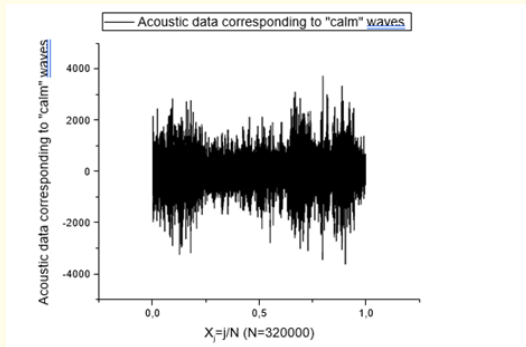**Figure 9:** This surface is based on the mantissa of maximal values corresponding to the non-filtered data.

Figure 10: This surface is based on the mantissa of maximal values corresponding to the filtered data. Comparison of these two surfaces shows that mantissa of the numbers is less sensitive in comparison with orders of corresponding numbers. Small differences are appeared in the distribution of the numeric values of these surfaces. Other surfaces based on mantissa of mean and minimal values, correspondingly, demonstrate the same behavior and, therefore, they are not shown.

**Analysis of acoustic data related to three types of waves.**

As the second example, we consider the acoustic signals associated with sea waves. We downloaded these acoustic signals from the site: "soundpunos.com". Unfortunately, we do not have some important details related to formation of these acoustic signals as waves, in particular, the place (fixed depth) of the Mediterranean Sea, where these acoustic signals were recorded, the wind force and is velocity and other parameters that lead to formation of the waves of the given intensity. We downloaded the signals for a "calm (cw) – (law intensity), "tranquil "(tw) – (mean intensity) and "storming"(sw) – (high intensity) waves, correspondingly. For us it is important only to highlight a certain "universality" of the method applied to transformation of the initial TLS into 3D-DGI surface based of the combined method described above.

Trendless Sequence as a New Source of Information: A Possibility to Present it in the Form of the Compact 3D-surface

33

Figure 11: Here we demonstrate the acoustic signal corresponding to "calm" sea containing $3.2 \cdot 10^5$ data points.
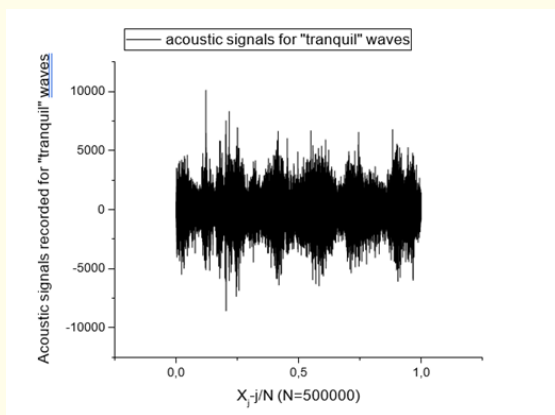
Figure 12: The acoustic signal corresponding to "tranquil" sea containing $5.0 \cdot 10^5$ data points.
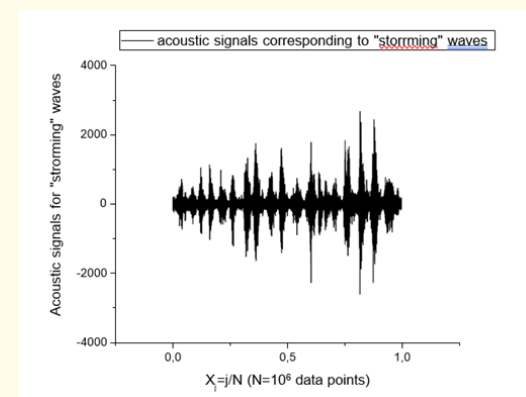
Figure 13: The acoustic signal corresponding to "storming" sea containing 106 data points. Comparison of these acoustic signals allows to notice the qualitative differences. In the "storming" state the waves concentrate their energy in the amplitudes of the high intensity, while for the waves that are in the "calm" and "tranquil" states the energy of the waves are "fuzzy" or "dissolved" over all amplitudes.

In figures 11-13 we show the original data that are obtained from transformation of "wav" acoustic files into the text files. It can be noticed that these original data contain interesting peculiarities. Comparison of these acoustic signals allows to notice the qualitative differences. In the "storming" state the waves concentrate their energy in the amplitudes of the high intensity, while for the waves that are in the "calm" and "tranquil" states the energy of the waves becomes "fuzzy" and dissolved over all amplitudes. How many 3D-surfaces can reflect the state of the waves if we transform the rectangle matrix ($N = 100 \times M = N_{band}/N$) to the matrix $P(P = 10) \times E$ (max(M), mean(M), min(M)) of the size ($10 \acute{} 3$)) containing only three columns? As it has been mentioned above for each column (if we represent each number as $Nm = e \times 10^d$) one can construct three surfaces (Nm, e, d) having different sensitivity. Therefore, each column will have three surfaces and each matrix will correspond to 9 surfaces. Finally, three matrices will give us 27 surfaces for more careful analysis. We cannot give them all and only 9 surfaces ($3\acute{}3$) for each selected wave (cw,tw,sw) corresponding to ten (Nm) numbers (p1-p10) will be given. Each parameter pi is located in the interval [min(pi), max(pi)]. These parameters are listed in Tables 3-5. The most significant parameters p_2, p_4, p_7 are bolded. The figures 14-16, 17-19, 20-22 demonstrate the surfaces for each type of waves (cw,tw,sw) correspondingly. As one can notice that comparison of surfaces corresponding to operational amplifiers with sea waves is different. The reason of this difference, from our point of view, is related to different contribution of parameters p_1-p_{10} related to construction of the last 9 surfaces. If the amplitudes become close to each other their values become more noticeable, while for the maximal and mean states the amplitudes distribution look more "poor". The surfaces corresponding to the values of mantissas (e) and orders (d) that were used for TLS(s) of OA(s) have another origin. Therefore, we obtain interesting option for visual presentation of trendless data or acoustic sea data (depicted in figures 14-22) with a "hidden" trend.

Results and Discussion

The analysis of various sources and recent works [21-25] related to this area shows that the topic related to a noise data processing becomes important today and finds wide application in solving various applied tasks related to signal processing and the construction of automated control systems.

In this paper we demonstrate the original combination of the previously developed methods as CAPoNeF [15] and 3D-DGI method [16] in one efficient "instrument" that allows to transform ini-

| Maximal values	Mean values	Minimal values
3.49103×10^2	-1.02392×10^0	-3.37257×10^2
7.17679×10^3	2.87457×10^3	1.18957×10^3
1.10198×10^3	-3.34270×10^1	-1.95165×10^3
1.130810^5	4.88655×10^4	1.69129×10^4
-5.06355×10^2	-1.43831×10^3	-3.56829×10^3
2.80000×10^1	-5.22293×10^{-1}	-3.00000×10^1
5.85497×10^2	2.54744×10^2	8.88471×10^1
1.28436×10^1	6.88132×10^0	2.40581×10^0
5.77567×10^0	2.27785×10^{-1}	-4.83263×10^0
1.42276×10^2	5.62900×10^1	6.00372×10^0

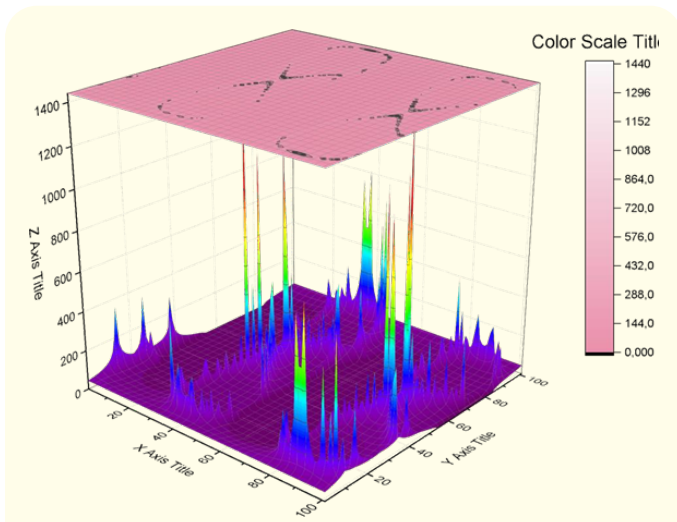**Table 3:** The key parameters p1-p10 corresponding to "calm" waves.
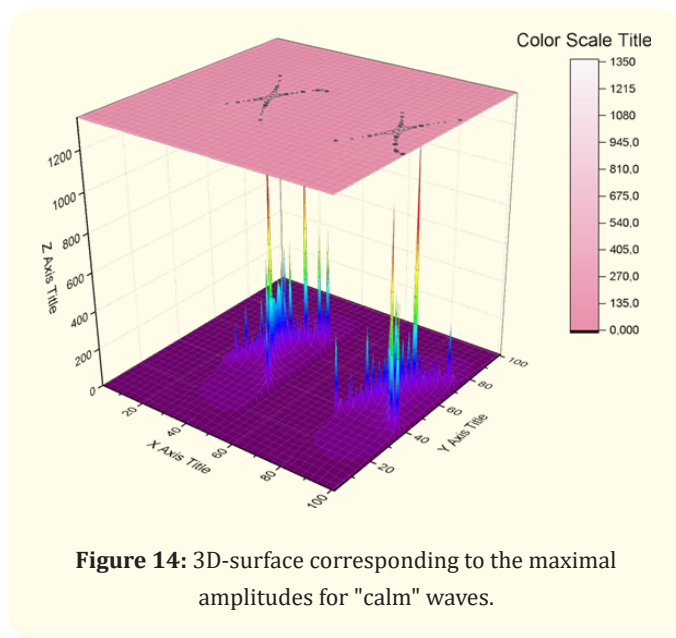
Figure 14: 3D-surface corresponding to the maximal amplitudes for "calm" waves.

| Maximal values	Mean values	Minimal values
1.49001×10^2	-4.63522×10^0	-1.21468×10^2
1.61104×10^4	7.20618×10^3	2.98412×10^3
4.95318×10^3	-1.22273×10^1	-2.69404×10^3
2.12010×10^5	1.03680×10^5	5.05657×10^4
-1.48311×10^3	-3.60772×10^3	-8.15029×10^3
1.20000×10^1	-7.17300×10^{-1}	-1.80000×10^1
1.11265×10^3	5.43346×10^2	2.65697×10^2
1.88315×10^0	1.12578×10^0	6.86864×10^{-1}
9.58175×10^{-1}	1.54240×10^{-2}	-8.10886×10^{-1}
2.43011×10^2	1.87150×10^2	1.25605×10^2

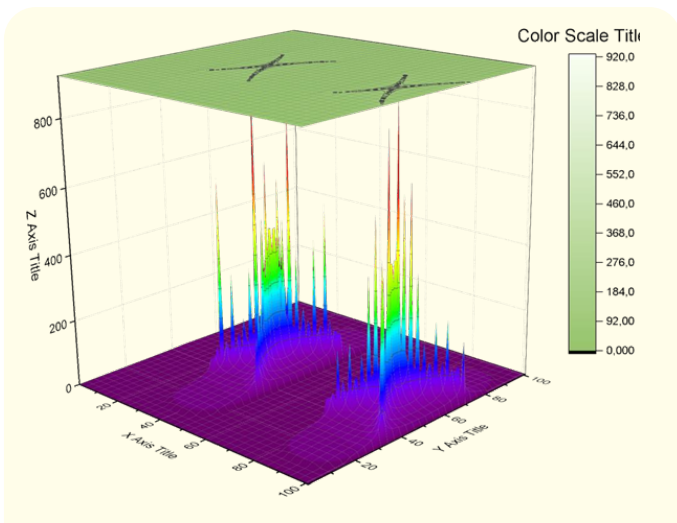**Table 4:** The key parameters p1-p10 corresponding to "tranquil" waves.
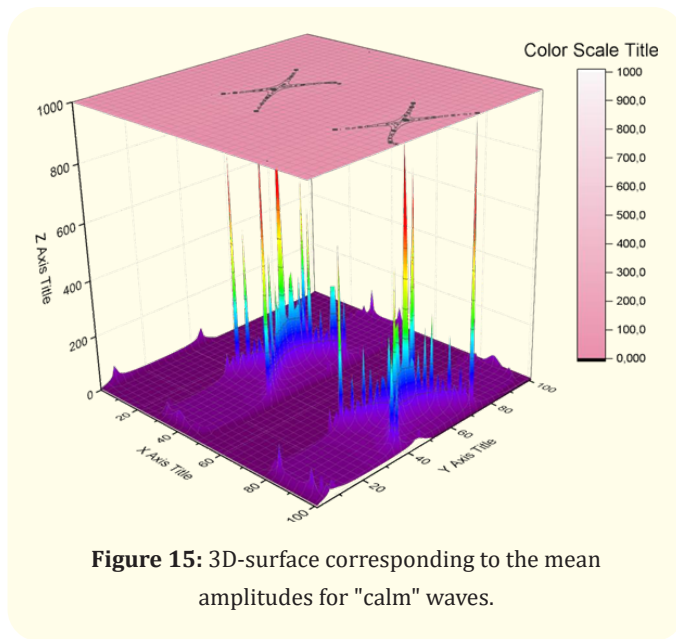
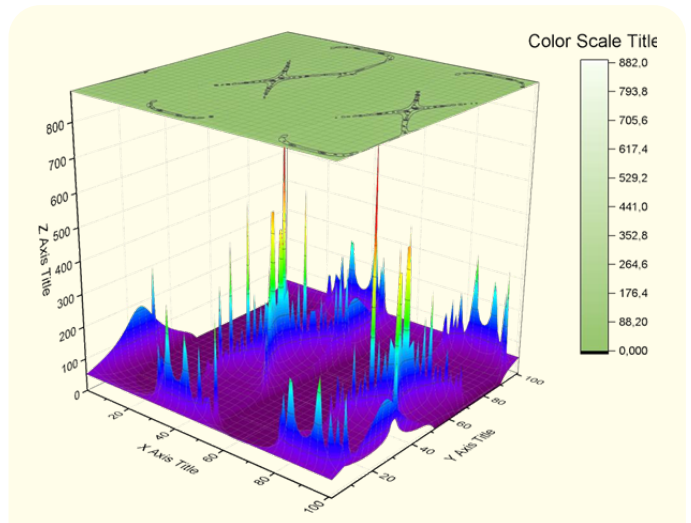**Figure 15:** 3D-surface corresponding to the mean amplitudes for "calm" waves.

Figure 16: 3D-surface corresponding to the minimal amplitudes for "calm" waves. Comparison of these three surfaces demonstrates clearly one peculiarity. More "rich" distribution of the amplitudes is observed for the surface corresponding to the minimal values. Their distribution of the heights shown on the right has the amplitudes with higher values in comparison with the surfaces with mean and maximal values.
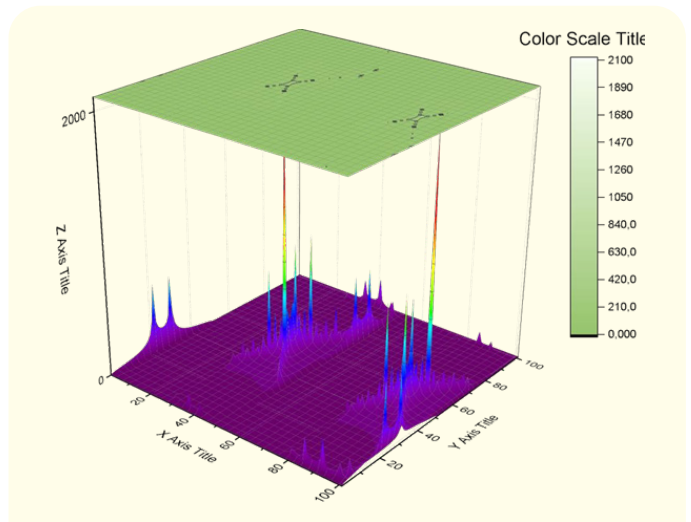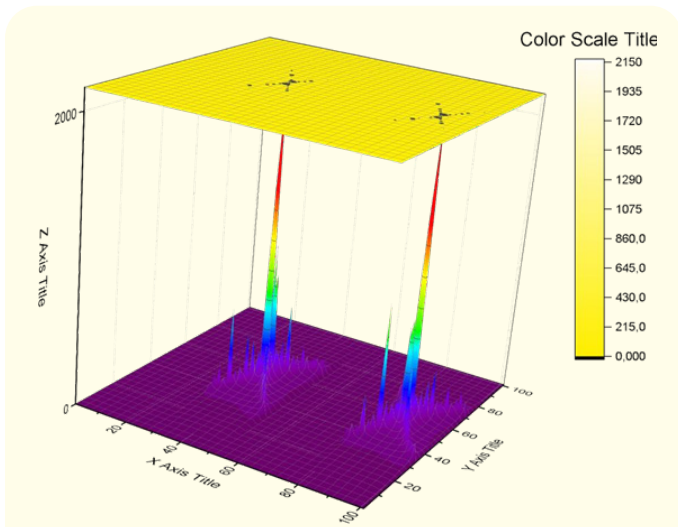

Figure 18: 3D-surface corresponding to the mean amplitudes for "tranquil" waves.
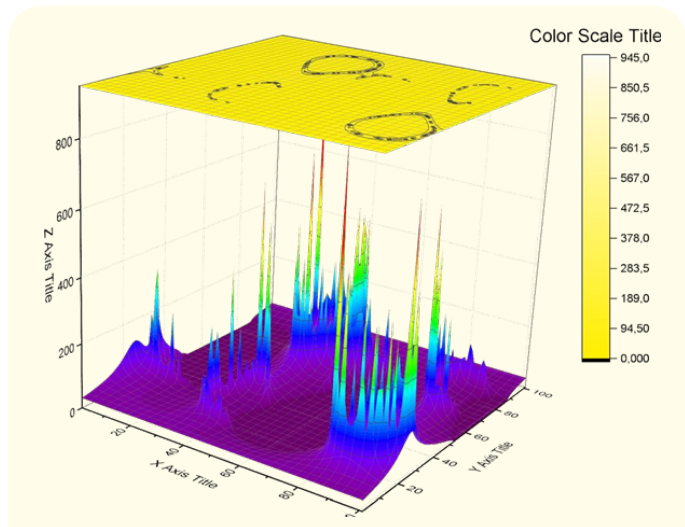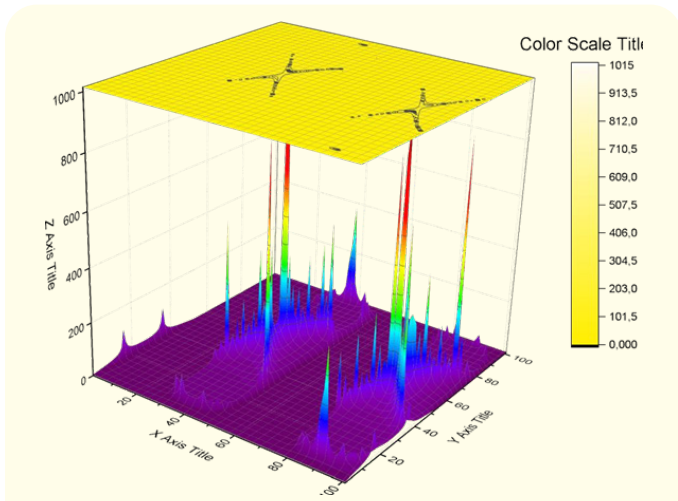

Figure 19: 3D-surface corresponding to the minimal amplitudes for "tranquil" waves. Comparison of the surfaces shown in figures 17-19 confirms the same peculiarity. More "rich" distribution of the amplitudes is observed for the surface corresponding to the minimal values.

Figure 17: 3D-surface corresponding to the maximal amplitudes for "tranquil" waves.

Figure 20: 3D-surface corresponding to the maximal amplitudes for "storming" waves.

Figure 22: 3D-surface corresponding to the minimal amplitudes for "storming" waves. Comparison of the surfaces shown in the previous figures confirms the same conclusion. More "rich" distribution of the amplitudes is observed for the surface corresponding to the minimal values.

Figure 21: 3D-surface corresponding to the mean amplitudes for "storming" waves.

Maximal values	Mean values	Minimal values
1.13039×10^2	-2.94312×10^{-1}	-7.87702×10^1
4.70306×10^3	9.70599×10^2	1.76178×10^2
1.16163×10^3	-3.06229×10^0	-9.85087×10^2
5.96314×10^4	1.33667×10^4	2.51879×10^3
-9.10990×10^1	-4.85594×10^2	-2.33242×10^3
1.60000×10^1	-5.20408×10^{-1}	-2.00000×10^1
3.14379×10^2	7.01898×10^1	1.32219×10^1
4.12472×10^0	1.79398×10^0	8.03985×10^{-1}
1.55555×10^0	3.08292×10^{-2}	-1.35269×10^0
2.38450×10^2	1.82863×10^2	1.30930×10^2

Table 5: The key parameters p1-p10 corresponding to "storming" waves.

Trendless Sequence as a New Source of Information: A Possibility to Present it in the Form of the Compact 3D-surface

37

tial rectangle matrix N(number of data points)×M (number of columns) to the compact matrix P(= 10 number of parameters)×E(= 3 extreme values). Then this compact matrix can be transformed to a finite set of 3D- surfaces. One can note that from one column of the matrix E, i.e. (max(M), mean(M), min(M)) one can receive at least three surfaces if one notice that any number forming a column can be written in the form $(N_m = e \times 10^d)$, where e is mantissa, d -is the order of the given number. The triple of numbers (Nm, e, d) – has different sensitivity and, therefore, the formed surfaces will have different forms.

These surfaces were applied to differentiation of filtered from nonfiltered data of the OAs. As it was turned out the surfaces formed from the orders (d) of from minimal and maximal values differentiate the filtered from nonfiltered data. The surfaces formed from mantissas have minimal differences.

As the second example we considered the marine acoustic data having hidden/(quasi-horizontal)trends. Application of the proposed method to these type of data helps to represent initial data in the visual forms (Figures 14-22).

We would like to stress again that initial "big data" contained matrices of the large dimensions $(N = 10^5\text{-}10^6) \times (M = 10^2\text{-}10^3)$ in many cases can be compressed to very compact matrices 10x3 with keepingof the influence of external factors that initially "dissolved" in "big data".

This paper is the first example of such kind. The authors will plan to apply this combination to other data, in particular, to "noisy" data related to production of chips and other devices, to detection of hacker attacks on the communications represented in the form of TLS(s), selection of the measuring device closest to the reference sample and etc.

Conclusion

In this final section we want to underline some key points that be associated with TLSs.

- Any big data represented in the form of rectangle matrices N×M can be reduced to matrices P(P = 10)x3.
- The reduced matrix can be presented in the form of 3D surfaces, having different sensitivities to the "hidden" external factors.

- The proposed method is universal and can be applied to any TLS. The selected 10 parameters are statistically significant and efficiency of the proposed methodology is demonstrated by the authors on available data.

Acknowledgements

Conflict of Interest

Authors declare no conflicts of interests.

Bibliography

1. Timashev S. "Flikker-noise spectroscopy. Information in Chaotic signals". 3rd ed.; Phys Mat Lit: Moscow, Russia, (2007): 1-248.

2. Timashev SF and Polyakov YuS. "Review of flicker noise spectroscopy in electrochemistry". *Fluctuations and Noise Letters* 7.2 (2007): 15-47.

3. Timashev SF., *et al*. "Uchenye Zapiski Kazanskogo Universiteta". *Seriya Fiziko-Matematicheskie Nauki* 154.4 (2012): 161-177.

4. Yulmetyev RM. "Stochastic dynamics of time correlation in complex systems with discrete time". *Physical Review E* 1 (2000): 6178-6194.

5. Yulmetyev RM. "Quantication of heart rate variability by discrete nonstationarity non-Markov stochastic processes". *Physical Review* 1 (2002): 046-107.

6. Nigmatullin RR and Vorobev AS. "The "universal" Set of Quantitative Parameters for Reading of the Trendless Sequences". *Fluctuation and Noise Letters* 18.4 (2019): 1950023.

7. Tyagai VA. "Faradaic noise of complex electrochemical reactions". *Electrochimica Acta* 16 (1971): 1647-1654.

8. Barker GC. "Faradaic reaction noise". *Journal of Electroanalytical Chemistry and Interfacial Electrochemistry* 82 (1977): 145-155.

9. Bozdech S., *et al*. "1/f2 noise in bistable electrocatalytic reactions on mesoscale electrodes". *Faraday Discussions* 193 (2016): 187-205.

10. Nigmatullin RR., *et al*. "New approach for PEMFC diagnostics based on quantitative description of quasi-periodic oscillations". *International Journal of Hydrogen Energy* 41 (2016): 12582-12590.

11. Astafev E. "Electrochemical noise measurements methodologies of chemical power sources". *Instrumentation Science and Technology* 47 (2019): 233-247.

12. Astafev E and Uksche A. "Peculiarities of hardware for electrochemical noise measurement in chemical power sources". *IEEE Transactions on Instrumentation and Measurement* 68 (2019): 4412-4418.

13. Gutenberg B., *et al*. "Seismicity of the Earth and associated phenomena". 3rd ed.;: Princeton University Press: Princeton, NJ, USA, (1949): 1-310.

14. Nigmatullin RR., *et al*. "Fractal description of the complex beatings: How to describe quantitatively seismic waves?" *Chaos, Solitons and Fractals* 120 (2019): 171-182.

15. Nigmatullin RR., *et al*. "Differentiation of Different Sorts of Sugars by the CAPoNeF Method". *Electroanalysis* 12 (2021): 1-8.

16. Nigmatullin RR. "Discrete Geometrical Invariants in 3D Space: How Three Random Sequences Can Be Compared in Terms of "Universal" Statistical Parameters?" *Frontiers in Physics* 14 (2020): 1-9.

17. Geng Yu P. "Analytic Acoustic-Elastic Coupled Equations and Their Application in Vector-Wave-Based Imaging of Ocean Bottom 4C Data". *Pure and Applied Geophysics* 177 (2020): 961-975.

18. Lepore S and Grad M. "Relation between ocean wave activity and wavefield of the ambient noise recorded in northern Poland". *Journal of Seismology* 24 (2020): 1075-1094.

19. Fokina MS and Fokin VN. "Numerical modeling of reflection coefficients of plane sound waves from a layered elastic bottom". *Acoustic Journal* 46.4 (2000): 551-559.

20. Saito T and Kawahara J. "Retrieval of long-wave tsunami Green's function from the cross-correlation of continuous ocean waves excited by far-field random noise sources on the basis of a first-order Born approximation". *Earth Planet* 1 (2012): 43-48.

21. Schillings C., *et al*. "On the convergence of the Laplace approximation and noise- level-robustness of Laplace-based Monte Carlo methods for Bayesian inverse problems". *Numerische Mathematik* 145 (2020): 915-971.

22. Fahim K., *et al*. "Some approximation results for mild solutions of stochastic fractional order evolution equations driven by Gaussian noise". *Stoch PDE: Anal CompScience* (2022).

23. von Hallern C and Rößler A. "A derivative-free Milstein type approximation method for SPDEs covering the non-commutative noise case". *Stoch PDE: Anal CompScience* (2022).

24. Schwalger T. "Mapping input noise to escape noise in integrate-and-fire neurons: a level-crossing approach". *Biological Cybernetics* 115 (2021): 539-562.

25. Bolin D., *et al*. "Weak convergence of Galerkin approximations for fractional elliptic stochastic PDEs with spatial white noise". *BIT Numerical Mathematics* 58 (2018): 881-906.